

# Mott physics and universal Planckian relaxation in the high- $T_c$ cuprates

A. Shekhter,<sup>1,\*</sup> B. J. Ramshaw,<sup>2</sup> M. K. Chan,<sup>1</sup> and N. Harrison<sup>1</sup>

<sup>1</sup>*Los Alamos National Laboratory, Los Alamos, NM 87545, USA*

<sup>2</sup>*Laboratory of Atomic and Solid State Physics, Cornell University, Ithaca, NY, USA*

(Dated: June 19, 2024)

Shortly after the discovery of high-temperature superconducting cuprates, Anderson proposed that Mott physics is instrumental in understanding their phase diagrams. Specifically, he suggested that, similar to the ‘almost-localized’ Fermi liquid in  $^3\text{He}$ , the effective mass renormalization in the cuprates is characteristic of a doped Mott insulator, scaling inversely with doping  $p$  away from half-filling. However, Mott physics has struggled to account for the ‘strange metal’ behavior, characterized by a linear-in-temperature ( $T$ ) ‘Planckian’ resistivity that extends to very high temperatures, casting doubt on the relevance of Mott physics in the cuprates. Here, we report a comprehensive survey of calorimetry and resistivity data spanning broad doping and temperature ranges. We find that the entropy at high temperatures closely adheres to that of an almost-localized Fermi liquid, implying that Mott physics remains relevant at high energies. We find that the strong doping dependence of the coefficient of the  $T$ -linear resistivity at high temperatures also scales inversely with  $p$ , suggesting a true universality of the Planckian relaxation rate across the entire phase diagram. Thus, the physics of the cuprates over their entire phase diagram is determined by the joint action of Mott physics and Planckian relaxation physics, with each operating at very different energy scales.

## INTRODUCTION

A central question in the study of high-transition-temperature ( $T_c$ ) superconducting cuprates is the origin of the ‘strange metal’ behavior, noted for its linear-in-temperature ( $T$ ) resistivity extending from high to low temperatures [1, 2]. It has been shown that the  $T$ -linear behavior of the resistivity extends over a broad range of dopings if measured at sufficiently high temperatures [3–7]. Recent suggestions indicate that the relaxation rate  $1/\tau$  is largely doping-independent [8], implying a universal (or ‘Planckian’) relaxation rate  $1/\tau_{\hbar}$  [9–12]:

$$\hbar/\tau_{\hbar} = \alpha k_{\text{B}}T \quad (1)$$

with  $\alpha \approx 1$  being weakly dependent on doping. However, such universality was demonstrated experimentally only over a narrow range of dopings near the ‘critical doping’  $p^* \approx 0.2$ . For Equation (1) to be truly universal (i.e., valid over the entire doping range), the entire doping dependence of the coefficient of the  $T$ -linear resistivity must be determined solely by the quasiparticle effective mass on the Fermi surface [8]. It is therefore imperative to thoroughly characterize and understand the behavior of this mass enhancement across the entire doping range.

The prevailing view links the strange metal to quantum criticality [13–23], associated with fluctuations of a distinct order parameter—a phenomenon well-documented in heavy fermion materials [24–28]. The universal appeal of this hypothesis in the cuprates is that it posits these fluctuations as the pairing glue. It has also been argued that these same fluctuations, which are strongest near the critical doping  $p^*$  at low enough temperatures, must also cause the mass enhancement [29–31]. Yet it has remained an open question whether the mass renor-

malization is itself determined by such fluctuations or has an independent origin.

It is interesting to note that a similar discussion once took place concerning the direct role of order parameter fluctuations in enhancing the effective mass in the Fermi liquid state of  $^3\text{He}$  [32, 33]. While it was initially believed that the pressure-dependent quasiparticle mass and Landau parameters in  $^3\text{He}$  were due to its proximity to a Stoner instability [34], it was subsequently shown that such an instability could not simultaneously account for the observed magnitude of the effective mass and magnetic susceptibility [35–37]. Instead, it was shown that Fermi liquid relations require the observed thermodynamic properties to be determined by an enhancement of the quasiparticle effective mass that occurs independently of magnetic fluctuations. The transformative idea that enabled a quantitative understanding of the pressure-dependent Fermi liquid parameters in  $^3\text{He}$  is that the enhancement of the quasiparticle effective mass is caused by the suppression of the mobility of  $^3\text{He}$  atoms by hard-core repulsive interactions. This is referred to as an ‘almost-localized Fermi liquid,’ in analogy with a Mott insulator doped away from half-filling by a small amount  $p$  [35–37].

To account for the strong short-range repulsion in  $^3\text{He}$ , Anderson and Vollhardt [35–37] introduced the lattice-gas model with on-site interaction  $U$ . Importantly, they recognized that the number of sites in the lattice model of  $^3\text{He}$  liquid differs from the number of atoms. Consequently, the liquid is described by a new thermodynamic parameter  $p$  (labeled  $\delta$  in their work), which exists alongside pressure and temperature, akin to an order parameter without symmetry breaking [40, 41]. This parameter defines a small difference between the volume per site of the lattice,  $v_{\text{s}}$ , and the volume per atom,  $v_{\text{a}}$ , expressed as

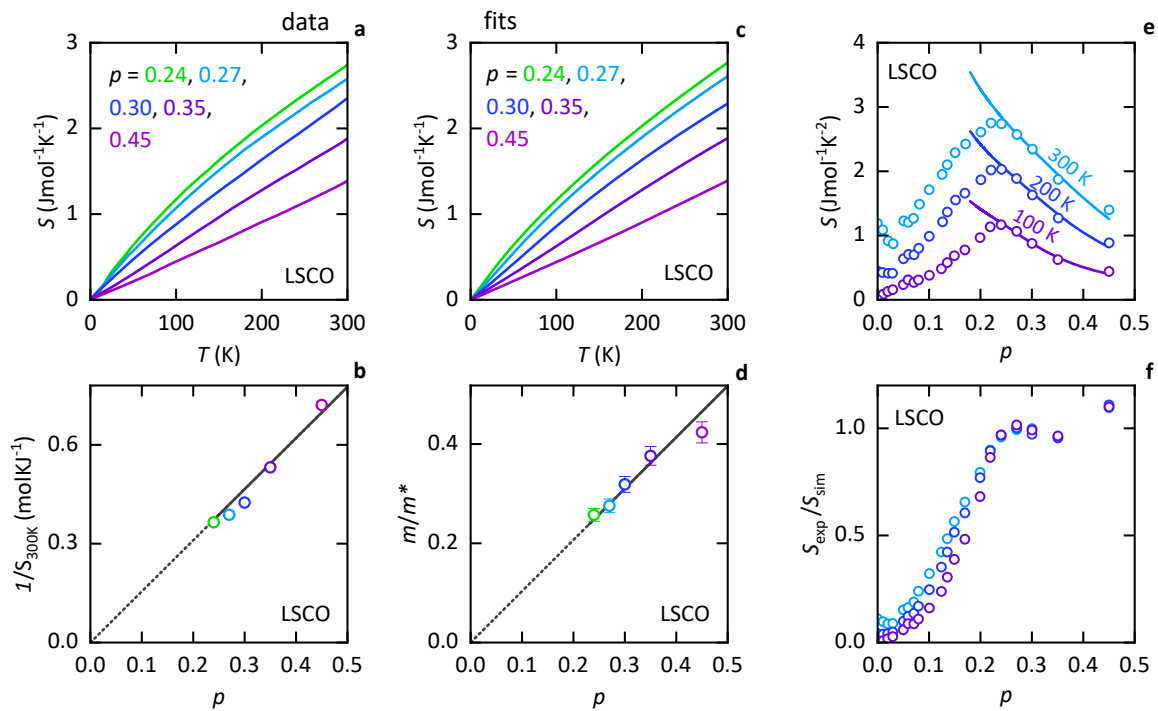


FIG. 1. **a**, Measured electronic contribution to the entropy  $S$  versus  $T$  of LSCO (see Appendix) at several hole dopings  $p$  [38]. **b**, Plot of  $1/S_{300\text{K}}$  (inverse electronic entropy at 300 K) versus  $p$  (the lines are rescaled from **d**). **c**, Simulated  $S$  versus  $T$  curves using fitted values of  $m/m^*$  from **d** and the tight-binding dispersion (see Appendix for details). **d**, Fitted values of  $m/m^*$  plotted versus  $p$ . The solid line corresponds to  $m/m^* = (1.03 \pm 0.02) \times p$ , with the error corresponding to the standard error of  $(1/p)(m/m^*)$ . The dotted line is the extrapolation of the solid line to  $p = 0$ . **e**, Measured entropy [39] (circles) at three different temperatures compared to that simulated (solid lines) using  $m/m^* = 1.03 \times p$  (see Appendix for details). **f**, Ratio of the experimentally measured electronic entropy [39]  $S_{\text{exp}}$  and simulated entropy  $S_{\text{sim}}$  (circles) from **e**.

$p = 1 - v_s/v_a$ ; essentially, it acts as an effective doping. Similar to the Landau description of phase transitions,  $p$  is determined by minimizing the free energy. While the Mott insulating state occurs at  $p = 0$ , it is preempted by solidification in  $^3\text{He}$  at  $p \approx 0.05$ , corresponding to a pressure of 34.36 bar [37, 41].

In the limit of strong hard-core repulsion, the effective mass enhancement in  $^3\text{He}$  is inversely proportional to the doping:  $m^*/m \approx 1/2p$  [36, 37]. Here,  $m$  corresponds to the mass of an isolated  $^3\text{He}$  atom, while  $m^*$  is the renormalized effective mass near the Fermi surface at temperatures well below the Fermi energy. Accordingly, the  $1/p$ -enhancement of the effective mass driven by hard-core repulsion at short distances is the hallmark of an almost-localized Fermi liquid.

A comprehensive understanding of the effective mass enhancement in  $^3\text{He}$  [35–37] was predicated on the Fermi liquid behavior of  $^3\text{He}$  at very low temperatures [32, 33]. We therefore begin our study of  $m^*/m$  in the cuprates from very high dopings, where they are established to be Fermi liquids at sufficiently low temperatures [42–46]. In the case of the cuprates,  $m$  refers to the band structure mass, calculated using a local density approximation that neglects electron correlation effects [47–49].

## RESULTS

In a Fermi liquid, the effective mass can be directly inferred from the electronic entropy  $S = \gamma T$  and the electronic specific heat coefficient  $\gamma = C/T = \partial S/\partial T$ , where  $C$  is the electronic specific heat and  $T$  is the temperature. In a layered metal,  $\gamma$  is related to  $m^*$  via  $\gamma = m^*(\pi k_B^2 N_A a^2/3\hbar^2) \approx m^*/m_e \times 1.4 \text{ J mol}^{-1}\text{K}^{-2}$  [45], with  $a$  being the in-plane lattice constant (see Appendix). In Fig. 1a, we plot the measured electronic entropy of the cuprate  $\text{La}_{2-x}\text{Sr}_x\text{CuO}_4$  (LSCO) [38, 39] over a wide range of temperatures and dopings (see Appendix for experimental details and plots of  $\gamma$ ).

Assuming Fermi liquid phenomenology [50], the electronic entropy  $S_{300\text{K}}$  at 300 K in Fig. 1a can be used to determine the electronic coefficient of specific heat, which in turn can be used to estimate the effective mass. Figure 1b shows that the inverse electronic entropy is proportional to  $p$  from  $p^*$  to  $p = 0.45$ , which implies that the effective mass is proportional to  $1/p$ .

Our reason for considering the entropy at highest accessible temperature is that it avoids the low-temperature deviation from linearity (see Fig. 1a), which we attribute to the proximity to a Van Hove singularity [51]. Our

detailed simulation, which incorporates the effect of the Van Hove singularity through an existing tight-binding approximation to the electronic dispersion [51] (see Appendix for details), is shown in Fig. 1c. This simulation produces  $m/m^*$  directly as a fitting parameter (plotted in Fig. 1d), whose value is independent of the Van Hove singularity. Both the qualitative estimate from  $S_{300\text{K}}$  and the quantitative analysis of the full temperature dependence yield:

$$m^*/m \approx 1/p. \quad (2)$$

Such behavior is the hallmark of an almost-localized Fermi liquid, as discussed by Vollhardt [36] for  $^3\text{He}$ . The approximate twofold larger factor for the mass renormalization in the LSCO cuprates was in fact proposed by Anderson using a different approximation to a doped Mott insulator [52, 53]. The  $p$ -inverse behavior of the quasi-particle mass at  $p > p^*$  in the Fermi liquid regime implies that the mass enhancement is predominantly governed by short-range, local repulsive interactions similar to those in  $^3\text{He}$  [52, 54–56].

Having shown that the physics of an almost localized Fermi liquid applies at dopings  $p > p^*$ , an important question concerns whether this physics extends into the underdoped regime  $p < p^*$ . If Mott physics extends into this regime [52], then the effective mass renormalization is expected to become much stronger. A difficulty with considering specific heat measurements at  $p < p^*$  is that the reduced Fermi velocity in the antinodal region of the Brillouin zone, relative to the nodal region, causes the specific heat of the Fermi liquid regime to be dominated by antinodal states. This leads to a dramatic reduction in the entropy relative to the simulated curve (see Fig. 1e) once these states become gapped by the pseudogap [39], which primarily affects the antinodal states [57]. Considering the ratio of the measured and simulated entropy in Fig. 1f, it is clear that the loss of entropy continues to be significant even at 300 K, which is the highest temperature to which it has been measured [39].

We can instead address the question of whether the physics of an almost localized Fermi liquid persists in the regime  $p < p^*$  by considering electrical resistivity measurements [6–8]. The electrical resistivity is dominated by nodal states, which have a higher mobility [11] and remain ungapped [57]. This enables the high-temperature limiting behavior of the resistivity to be accessed at lower temperatures than is possible with specific heat measurements.

Over a broad range of dopings and at sufficiently high temperatures, the electrical resistivity in the cuprates has been found to exhibit a  $T$ -linear behavior [3–7]. In LSCO, we find the  $T$ -linear behavior to occur above a doping-dependent crossover temperature,  $T_{\text{co}}$ , as shown in Fig. 2a (see Appendix). The coefficient of the  $T$ -linear resistivity,  $A = \partial\rho/\partial T$ , inferred from high-temperature

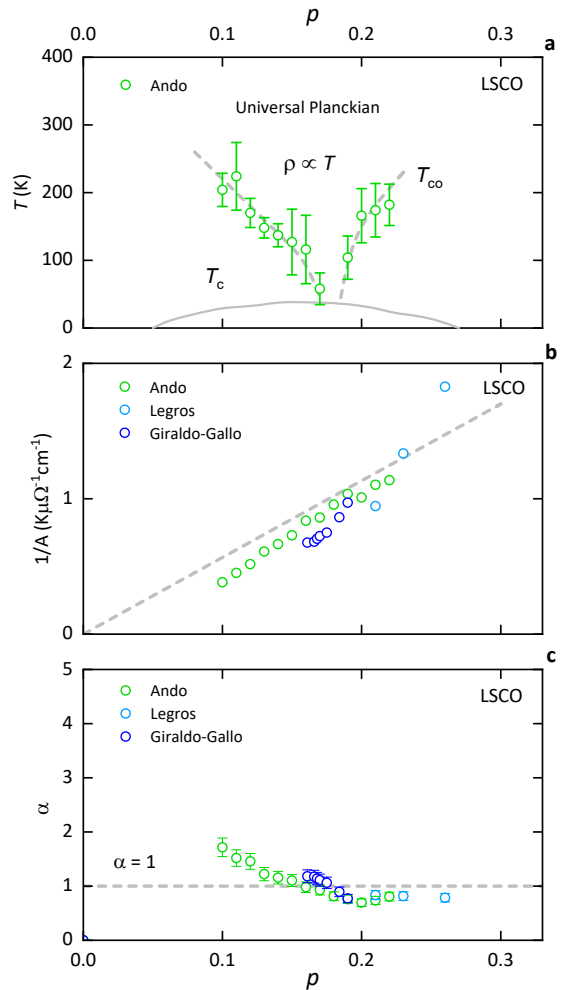


FIG. 2. **a**, Crossover temperature  $T_{\text{co}}$  above which  $\rho$  is  $T$ -linear determined from linear fits to LSCO resistivity measurements [6] (see Appendix for details). **b**,  $1/A$  versus  $p$  in LSCO from Ando *et al.* [6] determined using linear fits (see Appendix for details). Also included are  $1/A$  from Legros *et al.* [8] and Giraldo-Gallo *et al.* [7]. **c**, Estimates of  $\alpha$  according to a Drude approximation, using  $\alpha = A(e^2\hbar n/k_B m^*)$ , where  $m^*$  is obtained assuming  $m^* = \gamma/(\pi k_B^2 N_A a^2/3\hbar^2)$  [45] and the simulated  $\gamma$  for LSCO from Fig. 3a. For this purpose, it is sufficient to approximate the density with that of a half-filled band:  $n = 1/(a^2c)$  (see Appendix).

measurements, has also been found to increase with decreasing hole doping [3–7]. In LSCO, we find the doping dependence of the  $T$ -linear slope ( $A$ ) of the resistivity in the high-temperature regime to follow the same  $p$ -inverse law as the effective mass enhancement (see Fig. 2b).

Generally, the electrical resistivity in a correlated metal is considered starting from the Einstein relation [58, 59], where the conductivity is the product of the compressibility and diffusion constant on the Fermi surface. From this relation:  $\rho \approx m^*/ne^2 \times (1/\tau)$ , consistent with the simpler Drude approximation [8]. It is important to note that the density  $n$  here refers to the

total number of electrons (or holes), including the one electron per site in the half-filled band (see Fig. 2).

Figure 2b establishes that the slope of the  $T$ -linear resistivity follows a  $p$ -inverse law over the entire doping range, overlapping with the doping range  $p > p^*$  where the specific heat provides direct evidence for the mass following such a law. If one attributes the doping dependence of  $A$  entirely to the doping dependence of  $m^*$ , then this would extend the  $p$ -inverse law of  $m^*$  deep into the underdoped regime. The Planckian relaxation rate  $1/\tau_h$  must therefore be weakly doping-dependent across the entire doping range, i.e., truly universal. With this universality in mind and using  $n$  defined above, in Fig. 2c we use the slope  $A$ , together with  $m^*$  estimated from the simulated specific heat (see Fig. 3), to determine the doping dependence of the coefficient  $\alpha$  in Equation (1). The doping dependence of  $\alpha$ , as thus obtained, is close to unity over the entire doping range (see Appendix).

Given the continuous doping dependence of the slope of the  $T$ -linear resistivity across the critical doping and the universal character of the Planckian relaxation rate, we should scrutinize prior reports of an anomalously large effective mass near the critical doping [29–31].

We begin this discussion by considering low temperature specific heat measurements plotted in Fig. 3. Figures 3a & b show the doping dependences of the low-temperature electronic specific heat coefficient  $\gamma$  in LSCO [31], and in  $\text{La}_{2-y-x}\text{Nd}_y\text{Sr}_x\text{CuO}_4$  (Nd-LSCO) and  $\text{La}_{2-y-x}\text{Eu}_y\text{Sr}_x\text{CuO}_4$  (Eu-LSCO) [30], respectively. The sharp peak in the low-temperature specific heat coefficient has been interpreted as evidence for a mass enhancement near a quantum critical point. A quantum critical origin of the mass enhancement was further substantiated in the same work by the observation of a logarithmic temperature dependence of the electronic specific heat coefficient (Fig. 3c) [30].

Instead, the solid lines in Figs. 3a & b show that the doping and temperature dependences can be understood in their entirety by the model, which includes  $p$ -inverse behavior of the mass renormalization together with the Van Hove singularity [51]; the same model used in Figs. 1c and d without any further adjustments. The peak in  $\gamma$  in Nd-LSCO and Eu-LSCO [30] can be attributed entirely to the band effects associated with proximity to a Van Hove singularity (see schematic in Fig. 3d). This also applies to the logarithmic temperature dependence (see Fig. 3c). Hence, in all three systems the peaked contribution from the Van Hove singularity effectively rides on top of a dominant, smoothly varying  $p$ -inverse background driven by correlation effects [36, 37]; see illustration in Fig. 3d. In the case of LSCO, the direct observation of the Van Hove peak is preempted by the opening of the pseudogap. Also, because the singularity in  $\gamma$  is logarithmic in temperature, its effect on the entropy is strongly suppressed at high temperatures, causing  $S_{300\text{K}}$  in Fig. 1c to be largely unaffected. This is

why  $1/S_{300\text{K}}$  and  $m/m^*$  are very similar in Figs. 1c and d.

## DISCUSSION

From the very beginning [61], the discussion of the cuprates has been a standoff between two opposing views: one rooted in the physics of a Mott insulator at very high energies, and the other based on an abundance of empirical evidence for quantum criticality, mostly near  $p^*$  [2, 10, 20, 52, 56, 62–64]. Our finding of a  $p$ -inverse doping dependence of the effective mass renormalization provides direct evidence for Mott physics. Hence, the two opposing views cannot be considered in isolation but must together determine the observed behavior. The physical properties of the cuprates are governed by short-range Mott physics at high energies and by a universal Planckian relaxation rate associated with long-range fluctuations at very low energies. There is no longer a standoff between the opposing views if the Mott and Planckian mechanisms operate at very different energy scales and are thus described by entirely different principles [65]. Such a decoupling between the high and low energy physics is not without precedent: it was previously established in the Fermi liquid state of  $^3\text{He}$  [36, 37].

**Acknowledgements** We thank Ross McDonald for illuminating discussions. Work specific to the cuprates was performed as part of the Department of Energy (DoE) BES project ‘Science of 100 tesla.’ The entropy calculation procedures were developed as part of a LDRD DR project at Los Alamos National Laboratory. The National High Magnetic Field Laboratory is funded by NSF Cooperative Agreements DMR-1157490 and 1164477, the State of Florida and DoE. MKC acknowledges support from NSF IR/D program while serving at the National Science Foundation. Any opinion, findings, and conclusions or recommendations expressed in this material are those of the author(s) and do not necessarily reflect the views of the National Science Foundation.

---

\* email: [arkadyshekhter@gmail.com](mailto:arkadyshekhter@gmail.com)

- [1] S. Martin, A. T. Fiory, R. M. Fleming, L. F. Schneemeyer, and J. V. Waszczak, *Phys. Rev. B* **41**, 846 (1990).
- [2] P. W. Anderson, *Science* **256**, 1526 (1992).
- [3] H. Takagi, B. Batlogg, H. L. Kao, J. Kwo, R. J. Cava, J. J. Krajewski, and W. F. Peck, *Phys. Rev. Lett.* **69**, 2975 (1992).
- [4] T. Ito, K. Takenaka, and S. Uchida, *Phys. Rev. Lett.* **70**, 3995 (1993).
- [5] T. Watanabe, T. Fujii, and A. Matsuda, *Phys. Rev. Lett.* **79**, 2113 (1997).
- [6] Y. Ando, S. Komiya, K. Segawa, S. Ono, and Y. Kurita, *Phys. Rev. Lett.* **93**, 267001 (2004).

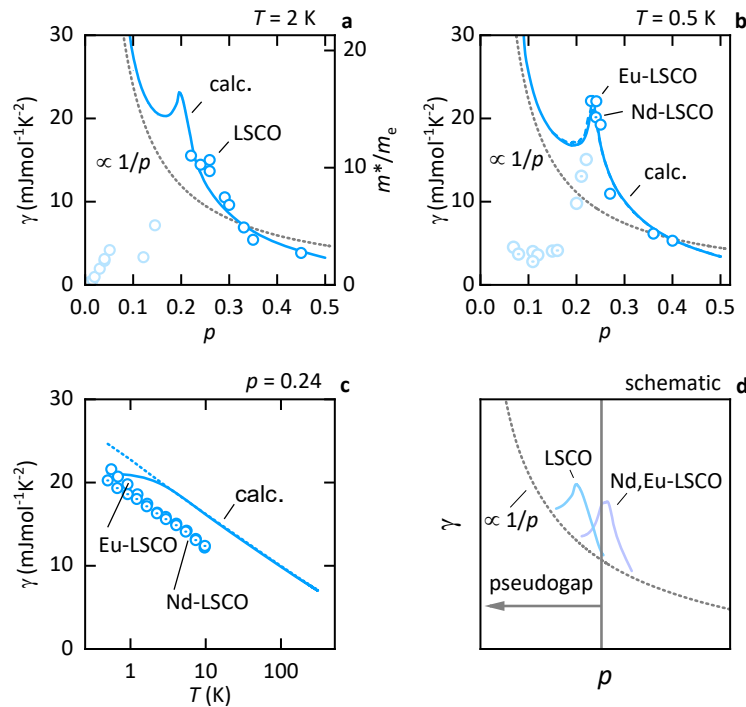


FIG. 3. **a**, Measured  $\gamma$  versus  $p$  at  $T = 2$  K for LSCO [31, 39] (circles) compared against that calculated using  $m/m^* = 1.03 \times p$  (lines) and a ratio of the interlayer hopping to the nearest neighbor in-plane hopping  $t_z/t$  of 0.07 [51] (solid line). Experimental points at  $p < 0.23$  are plotted in lighter blue for clarity. Note that for  $p \geq 0.3$ , the  $\gamma$  values are from Ref. 39. The right-hand axis shows the equivalent mass, estimated using  $\gamma \approx m^* \times 1.4 \text{ Jmol}^{-1} \text{K}^{-2}$  (see Appendix). The dotted grey line has been added to compare with  $\gamma$  expected in the absence of a Van Hove singularity. **b**, Measured  $\gamma$  versus  $p$  at  $T = 0.5$  K for Nd-LSCO and Eu-LSCO [30] (circles) compared against that calculated  $m/m^* = 1.03 \times p$  (lines) and a ratio of the interlayer hopping to the nearest neighbor in-plane hopping  $t_z/t$  of 0.07 [51] (solid line), and  $t_z/t$  of 0.03 [60] (dashed line). **c**, Measured  $\gamma$  versus  $T$  of Nd-LSCO and Eu-LSCO on a semilogarithmic scale at  $p = 0.24$  compared against calculated curves at  $p = 0.235$ , using  $t_z/t$  of 0.07 (solid line), and  $t_z/t$  of 0 (dotted line). See Appendix for details. **d**, Schematic showing contributions to  $\gamma$  from strong repulsive interactions (grey dotted curve  $\propto 1/p$ ) and the Van Hove singularities in LSCO and Nd- and Eu-LSCO (colored curves).

- [7] P. Giraldo-Gallo, J. A. Galvis, Z. Stegen, K. A. Modic, F. F. Balakirev, J. B. Betts, X. Lian, C. Moir, S. C. Riggs, J. Wu, A. T. Bollinger, X. He, I. Bozovic, B. J. Ramshaw, R. D. McDonald, G. S. Boebinger, and A. Shekhter, *Science* **361**, 479 (2018).
- [8] A. Legros *et al.*, *Nature Phys.* **15**, 142 (2019).
- [9] J. A. N. Bruin, H. Sakai, R. S. Perry, and A. P. Mackenzie, *Science* **339**, 804 (2013).
- [10] J. Zaanen, *SciPost Phys.* **6**, 061 (2019).
- [11] G. Grissonnanche, Y.-W. Fang, A. Legros, S. Verret, F. Laliberte, C. Collignon, J.-S. Zhou, D. Graf, P. A. Goddard, L. Taillefer, and B. J. Ramshaw, *Nature* **595**, 667 (2021).
- [12] S. A. Hartnoll and A. P. Mackenzie, *Reviews of Modern Physics* **94** (2022), 10.1103/RevModPhys.94.041002.
- [13] C. M. Varma, P. B. Littlewood, S. Schmitt-Rink, E. Abrahams, and A. Ruckenstein, *Phys. Rev. Lett.* **63**, 1996 (1989).
- [14] C. Castellani, C. Di Castro, and M. Grilli, *Phys. Rev. Lett.* **75**, 4650 (1995).
- [15] C. M. Varma, *Phys. Rev. B* **55**, 14554 (1997).
- [16] S. Chakravarty, R. B. Laughlin, D. K. Morr, and C. Nayak, *Phys. Rev. B* **63**, 094503 (2001).
- [17] S. A. Kivelson, I. P. Bindloss, E. Fradkin, V. Oganesyan, J. M. Tranquada, A. Kapitulnik, and C. Howald, *Rev. Mod. Phys.* **75**, 1201 (2003).
- [18] T. Senthil, A. Vishwanath, L. Balents, S. Sachdev, and M. P. A. Fisher, *Science* **303**, 1490 (2004).
- [19] A. Shekhter, B. J. Ramshaw, R. Liang, W. N. Hardy, D. A. Bonn, F. F. Balakirev, R. D. McDonald, J. B. Betts, S. C. Riggs, and A. Migliori, *Nature* **498**, 75 (2013).
- [20] B. Keimer, S. A. Kivelson, M. R. Norman, S. Uchida, and J. Zaanen, *Nature* **518**, 179 (2015).
- [21] L. Zhao, C. A. Belvin, R. Liang, D. A. Bonn, W. N. Hardy, N. P. Armitage, and D. Hsieh, *Nature Physics* **13**, 250 (2017).
- [22] Y. Sato, S. Kasahara, H. Murayama, Y. Kasahara, E.-G. Moon, T. Nishizaki, T. Loew, J. Porras, B. Keimer, T. Shibauchi, and Y. Matsuda, *Nat. Phys.* **13**, 1074 (2017).
- [23] S. Lederer, Y. Schattner, E. Berg, and S. A. Kivelson, *Proc. Natl. Acad. USA* **114**, 4905 (2017).
- [24] A. J. Millis, *Phys. Rev. B* **48**, 7183 (1993).
- [25] P. Gegenwart, Q. Si, and F. Steglich, *Nat. Phys.* **4**, 186 (2008).
- [26] P. Coleman, C. Pépin, Q. Si, and R. Ramazashvili, *J. Phys.: Condens. Matter* **13**, R723 (2001).
- [27] H. Shishida, R. Settai, H. Harima, and Y. Onuki, *J. Phys. Soc. Japan* **74**, 1103 (2005).

- [28] P. Coleman and A. J. Schofield, *Nature* **433**, 226 (2005).
- [29] B. J. Ramshaw, S. E. Sebastian, R. D. McDonald, J. Day, B. S. Tan, Z. Zhu, J. B. Betts, R. Liang, D. A. Bonn, W. N. Hardy, and N. Harrison, *Science* **348**, 317 (2015).
- [30] B. Michon *et al.*, *Nature* **567**, 218 (2019).
- [31] C. Girod, D. LeBoeuf, A. Demuer, G. Seyfarth, S. Imajo, K. Kindo, Y. Kohama, M. Lizaire, A. Legros, A. Gourgout, H. Takagi, T. Kurosawa, M. Oda, N. Momono, J. Chang, S. Ono, G.-Q. Zheng, C. Marcenat, L. Taillefer, and T. Klein, *Phys. Rev. B* **103**, 214506 (2021).
- [32] J. C. Wheatley, *Rev. Mod. Phys.* **47**, 415 (1975).
- [33] A. J. Leggett, *Rev. Mod. Phys.* **47**, 331 (1975).
- [34] S. Doniach and S. Engelsberg, *Phys. Rev. Lett.* **17**, 750 (1966).
- [35] P. W. Anderson and W. F. Brinkman, *The Helium Liquids: Proceedings of the Fifteenth Scottish Universities Summer School in Physics, 1974*, edited by J. Armitage and I. Farquhar, NATO Advanced Study Institutes (Academic Press, 1975).
- [36] D. Vollhardt, *Rev. Mod. Phys.* **56**, 99 (1984).
- [37] D. Vollhardt, P. Wölfle, and P. W. Anderson, *Phys. Rev. B* **35**, 6703 (1987).
- [38] J. L. Tallon and J. G. Storey, *Frontiers in Physics* **10**, 1030616 (2022).
- [39] J. W. Loram *et al.*, *J. Physics and Chemistry of Solids* **62**, 59 (2001).
- [40] A. F. Andreev and I. M. Lifshitz, *Soviet Physics JETP* **29**, 1107 (1969), *zh. Eksp. Teor. Fiz.* 56, 2057-2068 (June, 1969).
- [41] E. R. Grilly, *Journal of Low Temperature Physics* **4**, 615 (1971).
- [42] N. E. Hussey, M. Abdel-Jawad, A. Carrington, A. P. Mackenzie, and L. Balicas, *Nature* **425**, 814 (2003).
- [43] M. Plate, J. D. F. Mottershead, I. S. Elfimov, D. C. Peets, R. Liang, D. A. Bonn, W. N. Hardy, S. Chiuzbajian, M. Falub, and M. Shi, *Phys. Rev. Lett.* **95**, 077001 (2005).
- [44] B. Vignolle, A. Carrington, R. A. Cooper, M. M. J. French, A. P. Mackenzie, C. Jaudet, D. Vignolles, C. Proust, and N. E. Hussey, *Nature* **455**, 952 (2008).
- [45] P. M. C. Rourke, A. F. Bangura, T. M. Benseman, M. Matusiak, J. R. Cooper, A. Carrington, and N. E. Hussey, *New J. Phys.* **12**, 105009 (2010).
- [46] Y. Fang, G. Grissonnanche, A. Legros, S. Verret, F. Laliberté, C. Collignon, A. Ataei, M. Dion, J. Zhou, D. Graf, M. J. Lawler, P. A. Goddard, L. Taillefer, and B. J. Ramshaw, *Nat. Phys.* **18**, 558 (2022).
- [47] E. Pavarini, I. Dasgupta, T. Saha-Dasgupta, O. Jepsen, and O. K. Andersen, *Phys. Rev. Lett.* **87**, 047003 (2001).
- [48] L. F. Mattheiss, *Phys. Rev. Lett.* **58**, 1028 (1987).
- [49] D. J. Singh and W. E. Pickett, *Physica C* **C235-240**, 2113 (1994).
- [50] L. D. Landau, *Sov. Phys. JETP* **3**, 920 (1957).
- [51] M. Horio *et al.*, *Phys. Rev. Lett.* **121**, 077004 (2018).
- [52] P. W. Anderson, *Science* **235**, 1196 (1987).
- [53] Z. Zou and P. W. Anderson, *Physical Review B* **37**, 627 (1988).
- [54] M. Grilli and G. Kotliar, *Phys. Rev. Lett.* **64**, 1170 (1990).
- [55] P. A. Lee and N. Nagaosa, *Phys. Rev. B* **46**, 5621 (1992).
- [56] V. Emery and S. Kivelson, *Nature* **374**, 434 (1995).
- [57] T. Timusk and B. Statt, *Rep. Prog. Phys.* **62**, 61 (1999).
- [58] D. Pines and P. Nozieres, *Theory Of Quantum Liquids* (CRC Press, 1999).
- [59] A. M. Finkel'stein, *Z. Phys. B* **56**, 189 (1984).
- [60] Y. Zhong, Z. Chen, S.-D. Chen, K.-J. Xu, N. Hashimoto, Y. He, S.-K. Mo, and Z.-X. Shen, *Proc. Natl. Acad. USA* **119**, e2204630119 (2022).
- [61] J. G. Bednortz and K. A. Muller, *Z. Phys.* **64**, 189 (1986).
- [62] P. A. Lee, N. Nagaosa, and X.-G. Wen, *Rev. Mod. Phys.* **78**, 17 (2006).
- [63] J. R. Schrieffer and J. S. Brooks, eds., *Handbook of High-Temperature Superconductivity: Theory and Experiment* (Springer, 2007).
- [64] C. M. Varma, *Rev. Mod. Phys.* **92**, 031001 (2020).
- [65] P. W. Anderson, *Science* **177**, 393 (1972).
- [66] J. W. Loram *et al.*, *J. Superconductivity* **7**, 243 (1994).
- [67] W. F. Brinkman and T. M. Rice, *Phys. Rev. B* **2**, 4302 (1970).
- [68] G. Kotliar and J. Liu, *Phys. Rev. B* **38**, 5142 (1988).
- [69] J. M. Luttinger and J. C. Ward, *Phys. Rev.* **118**, 1417 (1960).
- [70] J. M. Luttinger, *Phys. Rev.* **119**, 1153 (1960).
- [71] M. K. Chan, N. Harrison, R. D. McDonald, B. J. Ramshaw, K. A. Modic, N. Barisic, and M. Greven, *Nature Commun.* **7**, 12244 (2016).
- [72] O. Andersen, A. Liechtenstein, O. Jepsen, and F. Paulsen, *Journal of Physics and Chemistry of Solids* **56**, 1573 (1995), proceedings of the Conference on Spectroscopies in Novel Superconductors.
- [73] F. Rullier-Albenque, H. Alloul, F. Balakirev, and C. Proust, *Europhysics Letters* **81**, 37008 (2008).
- [74] S. Musser, D. Chowdhury, P. A. Lee, and T. Senthil, *Phys. Rev. B* **105**, 125105 (2022).
- [75] J. M. Wade, J. W. Loram, K. A. Mirza, J. R. Cooper, and J. L. Tallon, *Journal of Superconductivity* **7**, 261 (1994).
- [76] S. E. Sebastian, N. Harrison, and G. G. Lonzarich, *Rep. Prog. Phys.* **75**, 102501 (2012).
- [77] D. Shoenberg, *Magnetic Oscillations in Metals* (Cambridge University Press, 1984).
- [78] A. Damascelli, Z. Hussain, and Z.-X. Shen, *Rev. Mod. Phys.* **75**, 473 (2003).
- [79] N. Barisic, S. Badoux, M. K. Chan, C. Dorow, W. Tabis, B. Vignolle, Y. Guichan, J. Beard, X. Zhao, and C. Proust, *Nature Phys.* **9**, 761 (2013).
- [80] B. S. Tan, N. Harrison, Z. Zhu, F. Balakirev, B. J. Ramshaw, A. Srivastava, S. A. Sabok-Sayr, B. Dabrowski, G. G. Lonzarich, and S. E. Sebastian, *Proc. Natl. Acad. USA* **112**, 9568 (2015).
- [81] S. E. Sebastian, N. Harrison, M. M. Altarawneh, C. H. Mielke, R. Liang, D. A. Bonn, W. N. Hardy, and G. G. Lonzarich, *Proc. Natl. Acad. USA* **107**, 6175 (2010).
- [82] M. R. Norman, J. Lin, and A. J. Millis, *Phys. Rev. B* **81**, 180513 (2010).
- [83] D. LeBoeuf, N. Doiron-Leyraud, B. Vignolle, M. Sutherland, B. J. Ramshaw, J. Levallois, R. Daou, F. Laliberté, O. Cyr-Choinière, J. Chang, Y. J. Jo, L. Balicas, R. Liang, D. A. Bonn, W. N. Hardy, C. Proust, and L. Taillefer, *Phys. Rev. B* **83**, 054506 (2011).
- [84] A. Shekhter, K. A. Modic, R. D. McDonald, and B. J. Ramshaw, *Phys. Rev. B* **95**, 121106 (2017).

## APPENDIX

**The measured electronic contribution to  $S$  in Fig. 1.** The most detailed description of the differential calorimetry method used to extract the electronic contribution to  $S$  and  $\gamma$  is provided in Ref. 66. The differential method involves the use of Zn doping to alter the electronic contribution while leaving the phonon contribution largely unchanged. While this method was originally applied to Y123, the same method has been applied to other cuprates, including LSCO [38].

**Tight-binding electronic dispersion used in calculating  $S$ .** Throughout, we assume the tight-binding approximation to the electronic dispersion to be renormalized by  $m/m^*$  [67, 68] so that

$$\begin{aligned} \epsilon_k = & \frac{m}{m^*} \left[ -2t(\cos(ak_x) + \cos(ak_y)) \right. \\ & + 4t' \cos(ak_x) \cos(ak_y) - 2t''(\cos(2ak_x) + \cos(2ak_y)) \\ & + 4t'''(\cos(ak_x) \cos(2ak_y) + \cos(ak_y) \cos(2ak_x)) \\ & + 2t_z \cos(ak_x/2) \cos(ak_y/2) [\cos(ak_x) - \cos(ak_y)]^2 \\ & \left. \times \cos(ck_z) \right] + \mu. \end{aligned} \quad (3)$$

Here,  $k_x$ ,  $k_y$ , and  $k_z$  represent components of the reciprocal lattice vector,  $a$  is the planar lattice spacing,  $c$  is the interlayer lattice spacing, and  $\mu$  is the chemical potential, adjusted to produce an unreconstructed Fermi surface cross-section comprising  $1 + p$  carriers, consistent with Luttinger's theorem [69, 70]. We use the nearest neighbor hopping,  $t = 430$  meV, as determined for the bare conduction band by electronic structure calculations [47–49], and ratios  $t'/t$ ,  $t''/t'$ , and  $t_z/t$  that are fixed. These ratios have been determined elsewhere [51] and are listed in Table I.

**Calculating  $S$  in Fig. 1.** Starting from Luttinger's discussion of Fermi liquid thermodynamics [69, 70], we adopt the approximation in which the quasiparticle relaxation rate is neglected; a reasonable assumption in the overdoped cuprates where  $A$  is smallest and  $T_{co}$  is large (see Fig. 2). The electronic density of states per copper oxide plane is therefore

$$\rho(E) = 2a^2 \int \frac{d^2k}{(2\pi)^2} \delta(\epsilon_k - E). \quad (4)$$

Here, the prefactor of 2 corresponds to the number of spins, and  $\delta(\epsilon_k - E)$  is a delta function defined such that  $\int \rho(E) dE = 2$ . The entropy is then given by [69, 70]:

$$S = N_A \int_{-\infty}^{\infty} dE \rho(E) [n_F \ln n_F + [1 - n_F] \ln(1 - n_F)], \quad (5)$$

where  $n_F = 1/(1 + \exp\{E/k_B T\})$  is the Fermi-Dirac distribution, and  $N_A$  is Avogadro's number.

Cuprate	$t'/t$	$t''/t'$	$t'''/t''$	$t_z/t$
LSCO	0.12	0.50	0	0.07
Nd-LSCO	0.14	0.50	0	0.07
Eu-LSCO	0.14	0.50	0	0.07
Hg1201	0.228	0.762	0.25	-
Y123	0.32	0.5	0	-
Y124	0.32	0.5	0	-

TABLE I. Ratios of hopping parameters for various cuprates [51, 71, 72].

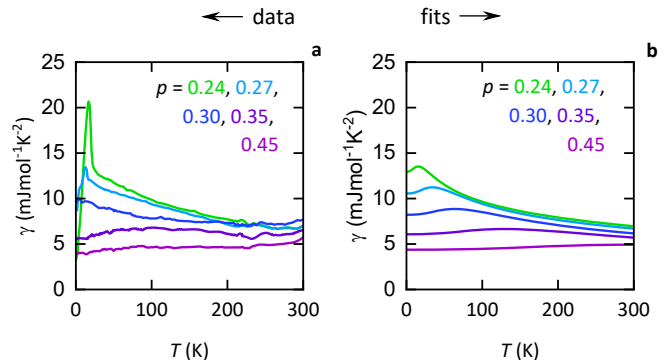


FIG. 4. **a**, Measured electronic coefficient  $\gamma$  of the specific heat. **b**, Calculated  $\gamma$  versus  $T$  curves using fitted values of  $m/m^*$ .

**Fitting  $m/m^*$ .** Using the above fixed values of  $t$  and the ratios  $t'/t$ ,  $t''/t'$ , and  $t_z/t$ , we calculate the entropy in Fig. 1c using Equation (5). Parity with the experimentally measured entropy in Fig. 1a is achieved by adjusting  $m/m^*$  in Equation (3). The resulting values of  $m/m^*$  are plotted in Fig. 1d. The errors are estimated from the small deviation of the calculated curve from the experimental curve.

#### The electronic specific heat versus temperature.

Figs. 4a and b show the measured [39] and calculated  $\gamma$  versus  $T$  curves, respectively. In the calculated curves, the Van Hove singularity gives rise to a weak maximum in  $\gamma$  as a function of temperature. While the Van Hove singularity accounts for the overall trends in  $\gamma$  versus  $T$  and  $p$ , the maximum itself appears to be visible in the experimental data only at  $p = 0.35$ . At  $p = 0.24$  and  $0.27$ , it is rendered unobservable by the superconducting anomaly. While the measurements of  $\gamma$  are affected by experimental noise, this is mostly integrated out when we consider the entropy in Fig. 1a and c.

**Fits to determine  $A$  and  $T_{co}$  in Fig. 2 from the measured resistivity.** To establish whether the data is well described by a  $T$ -linear behavior at high temperatures, in Fig. 5 we fit the function  $\rho = \rho_0 + AT$  to the in-plane resistivity data in LSCO [6] above 250 K for each hole doping. While this temperature is chosen arbitrarily, we find that the linear regression continues to

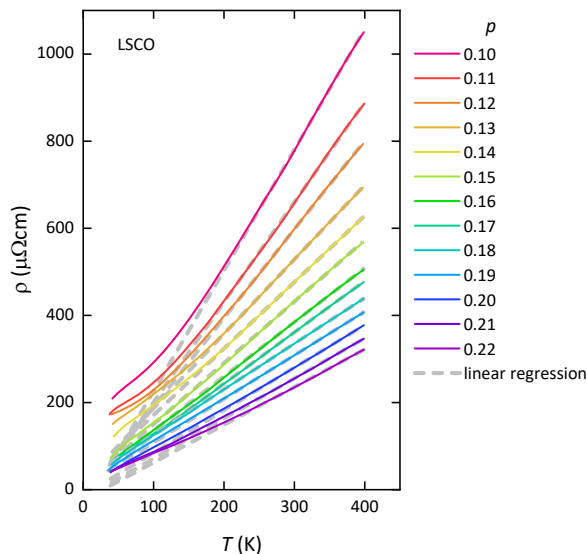


FIG. 5. Measured  $\rho$  versus  $T$  at different hole dopings [6], as indicated in different colors. Dashed lines indicate fits to determine  $A$ . The obtained values of  $1/A$  are plotted in Fig. 2b.

describe the data for a range of temperatures below this value. At  $p = 0.18$ , the  $T$ -linear behavior extends all the way from 400 K down to  $T_c$ . We define the crossover temperature  $T_{co}$  as the characteristic temperature below which the resistivity deviates from linearity. We choose  $3 \mu\Omega\text{cm}$  as the threshold above which a deviation from linearity is considered significant and estimate the error in  $T_{co}$  by increasing the threshold to  $10 \mu\Omega\text{cm}$ .

The downward departure of  $1/A$  from the dashed line below  $p \approx 0.15$  in Fig. 2b could arise either from a larger effect of the pseudogap at lower dopings or from a larger crossover temperature at these dopings (see Fig. 2a). It is also well-known that at these lower dopings, disorder effects are prevalent [73], leading to a glassy behavior approaching  $p \sim 0.05$ .

**Carrier density and mass values used in estimating  $\alpha$  in Fig. 2c.** Rather than considering the change in the Fermi surface from hole-like to electron-like at the Van Hove singularity, we have assumed  $n$  to be approximately constant:  $n = 1/(a^2c)$ , where  $a \approx 3.87 \text{ \AA}$  and  $c \approx 13.2 \text{ \AA}$  are the lattice parameters. Accounting for the change in density of the form  $1 + p$  or  $1 - p$  [8] as well as more realistic band structure parameters will only result in a change in  $\alpha$  of around 10%, which is not significant for the rough estimate in this paper. To improve upon this estimate, one will need to account for the above effects and consider a realistic pseudogap model. In the case of  $m^*$ , we have estimated this from  $\gamma$  at 2 K using the conversion  $\gamma = m^*(\pi k_B^2 N_A a^2 / 3\hbar^2) \approx m^*/m_e \times 1.4 \text{ J mol}^{-1} \text{ K}^{-2}$  [45].

**Effect of interlayer hopping on  $\gamma$  in the vicinity of the Van Hove singularity in Fig. 3c.** At

temperatures below  $\sim 2 \text{ K}$ ,  $\gamma$  in Fig. 3c becomes sensitive to the interlayer hopping. Whereas Ref. 51 finds  $t_z/t = 0.07$ , Ref. 60 finds  $t_z/t = 0.03$ . The measurements of  $\gamma$  close to  $p = 0.23$  were performed under strong magnetic fields [30]. It has been argued that orbital-averaging leads to a suppression of the interlayer hopping [74], which could cause the effective ratio  $t_z/t$  to drop to a significantly smaller value. For  $t_z/t = 0$ , the logarithmic divergence in Fig. 3c continues down to  $T = 0$ .

Scattering from defects introduces a residual scattering rate at  $T = 0$ , which can also cause  $\gamma$  to saturate. Angle-dependent magnetoresistance measurements have found the residual scattering rate to be momentum-dependent [11]. However, since the Fermi velocity vanishes along all momentum directions at the point of the Fermi surface where the Van Hove singularity occurs, angle-dependent magnetoresistance measurements are unable to constrain a value for this scattering rate at this point on the Fermi surface [11]. In order for the mean free path to remain non-vanishing at this point,  $\tau^{-1}$  must vanish at this point.

**The specific heat of Tl2201.** Specific heat measurements have been performed on  $\text{Tl}_2\text{Ba}_2\text{CuO}_6$  (Tl2201) [75] over a much narrower range of hole dopings than LSCO (see Fig. 6). Here, we have used values of the doping-dependent band mass  $m$  in Ref. 45 to simulate a curve of  $\gamma$  versus  $p$ . We first estimate  $m^*$  using  $m^*/m = 1.03/p$  (i.e., using the same dependence on  $p$  as obtained in Fig. 1d). Next, we calculate  $\gamma$  using  $\gamma = m^*(\pi k_B^2 N_A a^2 / 3\hbar^2) \approx m^*/m_e \times 1.4 \text{ J mol}^{-1} \text{ K}^{-2}$  [45]. Owing to the combined effect of the  $1/p$  scaling of  $m^*$  and the occurrence of the Van Hove singularity at much higher dopings in Tl2201 [43] than LSCO, the simulated  $\gamma$  is weakly dependent on  $p$  over the range in  $p$  where specific heat measurements have been made.

It should be noted that the phonon contribution used for extracting  $\gamma$  in Tl2201 was estimated from a non-superconducting composition at higher hole dopings rather than by performing additional measurements on samples in which Cu was substituted with Zn. This causes the doping dependence of the extracted  $\gamma$  curves in Tl2201 to be reliable only at the high and low temperature limits [75]. It is for this reason that the normal state values of  $\gamma$  plotted in Fig. 6a are for  $T = 200 \text{ K}$ .

**Comparison with magnetic quantum oscillation measurements.** We also consider the effective mass as determined from quantum oscillations. The mass measured at high dopings is consistent with the almost-localized Fermi liquid picture. Figure 6a shows  $m^*/m$  determined from measurements in Tl2201 [45], where  $m$  refers to the bare band mass specific to Tl2201 [45].

Quantum oscillation measurements in the underdoped regime, by contrast, pertain to small reconstructed sections of the Fermi surface comprising a number of carriers much smaller than  $1 + p$  [76]. A direct comparison of the measured effective mass with that in overdoped Tl2201



is therefore uninformative.

One might still be able to make a comparison by considering the orbitally-averaged Fermi velocity  $v_{\text{orb}}^* = \sqrt{2e\hbar F}/m^*$  from quantum oscillation measurements, where  $F$  is the quantum oscillation frequency [77]. This is because the Fermi velocity  $v_F = p_F/m$  along the nodal directions is believed to be only weakly affected by the pseudogap phenomenon [20, 78]. In such a case, the renormalized velocity  $v_F^* = p_F/m^*$ , assuming Luttinger's theorem [69, 70], provides a more reliable indicator of the underlying mass enhancement. Because the velocity away from the nodal directions is smaller than  $v_F^*$ ,  $v_F^*$  provides only an upper bound for the orbitally-averaged value; hence  $v_F^*/v_F \geq v_{\text{orb}}^*/v_F$ . All of the data from Refs. 29, 71, 79–81 in Fig. 6b fall close to or below the  $v_F^*/v_F \approx p$  line (see Appendix).

The values of  $v_F$  used in determining the ratio  $v_{\text{orb}}^*/v_F$  are obtained by calculating the band velocity  $v = \frac{1}{\hbar} \frac{\partial \epsilon_k}{\partial k}$  of the bare conduction band, at the point on the Fermi surface along the nodal direction. Using the hopping param-

eters for the tight-binding dispersion, we obtain  $v_{\{\text{node}\}} = 7.2 \times 10^5 \text{ ms}^{-1}$ ,  $6.6 \times 10^5 \text{ ms}^{-1}$  and  $6.6 \times 10^5 \text{ ms}^{-1}$  for Hg1201, Y123, and Y124, respectively. This velocity does not depend strongly on  $p$ .

Since  $v_F^*/v_F \approx p$  (dashed line in Fig. 3b) represents only an upper bound and quantum oscillations are measured at temperatures similarly low to those of the specific heat in Figs. 3a and b, the observed values of  $v_{\text{orb}}^*/v_F$  below this dashed line, as in the case of  $\text{YBa}_2\text{Cu}_3\text{O}_{6+x}$  (Y123) [29] (Y123<sup>a</sup> in Fig. 3b), do not contradict our findings. For example, the significant folding of the Brillouin zone required to produce small pockets can also produce Van Hove singularities in the reconstructed band structure, leading to an increase in the effective mass at low temperatures in the vicinity of a Lifshitz transition [82, 83]. It has further been suggested that quantum fluctuations can directly affect the temperature dependence of the quantum oscillation amplitude via the anomalous self-energy, causing the Lifshitz-Kosevich fitting to overestimate  $m^*$  [84]. Whether this is the case requires a more careful quantitative study of this effect.

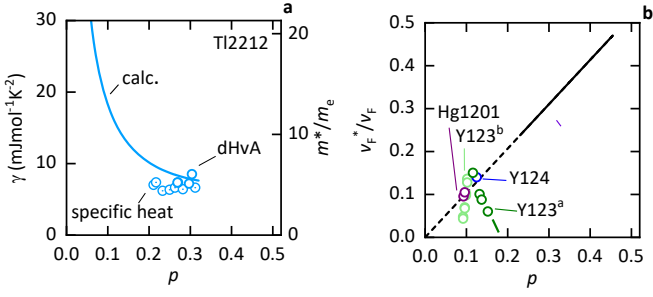


FIG. 6. **a**, Measured  $\gamma$  versus  $p$  at  $T = 200$  K for Tl2201 [75] (dot-centered circles) compared against  $\gamma$  simulated using  $m/m^* = 1.03 \times p$  (lines) and the calculated  $p$ -dependent band mass  $m$  from Ref. 45. Also shown are  $m^*/m_e$  values (open circles) obtained from de Haas-van Alphen (dHvA) measurements in overdoped Tl2201 [45]. Here, again, we assume  $\gamma = m^*(\pi k_B^2 N_A a^2 / 3\hbar^2) \approx m^*/m_e \times 1.4 \text{ J mol}^{-1} \text{ K}^{-2}$  [45]. **b**, The ratio of the orbitally-averaged Fermi velocities  $v_{\text{orb}}^*$  inferred from quantum oscillation measurements of small pockets to the nodal Fermi velocity  $v_F$  of the bare conduction band (see Appendix). Data are shown for YBa<sub>2</sub>Cu<sub>3</sub>O<sub>6+x</sub> (Y123) from Ref. 29 (Y123<sup>a</sup>) and Ref. 81 (Y123<sup>b</sup>), HgBa<sub>2</sub>CuO<sub>4+ $\delta$</sub>  (Hg1201) from Refs. 71 and 79, and YBa<sub>2</sub>Cu<sub>3</sub>O<sub>8</sub> (Y124) from Ref. 80. The green line is a guide to the eye. The black solid and dashed lines correspond to  $m/m^* = 1.03 \times p$  and  $v_{\text{orb}}^*/v_F = 1.03 \times p$ , respectively.